Superradiance, Disorder, and the Non-Hermitian Hamiltonian in Open Quantum Systems

G. L. Celardo*, A. Biella*, G. G. Giusteri*, F. Mattiotti*, Y. Zhang† and L. Kaplan†

*Dipartimento di Matematica e Fisica and Interdisciplinary Laboratories for Advanced Materials Physics, Università Cattolica, via Musei 41, 25121 Brescia, Italy
†Department of Physics and Engineering Physics, Tulane University, New Orleans, Louisiana 70118, USA

Abstract. We first briefly review the non-Hermitian effective Hamiltonian approach to open quantum systems and the associated phenomenon of superradiance. We next discuss the superradiance crossover in the presence of disorder and the relationship between superradiance and the localization transition. Finally, we investigate the regime of validity of the energy-independent effective Hamiltonian approximation and show that the results obtained by these methods are applicable to realistic physical systems.

Keywords: Open Quantum System, Non-Hermitian Hamiltonian, Superradiance, Localization
PACS: 73.23.-b, 05.60.Gg, 72.15.Rn

1. INTRODUCTION: OPEN SYSTEMS, NON-HERMITIAN EFFECTIVE HAMILTONIANS, AND SUPERRADIANCE

Open quantum systems are at the center of many research fields in physics today, ranging from quantum computing to transport in nano- and meso-scale solid state systems as well as in biological aggregates. In particular, charge/excitation transport in the quantum coherent regime can be considered one of the central subjects in modern solid state physics [1, 2].

When a discrete quantum system is very weakly coupled to a continuum, e.g. via tunneling to a decay channel or lead, the coupling may be treated perturbatively. In this regime, the closed system eigenstates become non-overlapping resonances, with all resonance widths proportional to the strength of the coupling. As the coupling grows, however, a rearrangement eventually occurs in which a subset of resonances, equal in number to the open channels, continue to grow in width, while the remaining resonances become trapped within the system. This rearrangement is known as the superradiance crossover, in analogy with Dicke superradiance for atoms interacting coherently with an electromagnetic field [3]. The two sets of resonances are known as the superradiant and subradiant states, respectively. In the limit of very strong coupling (where the energy scale is set by the Hamiltonian of the original closed system), all of the decay width is shared by the superradiant states (which approach "doorway" states in this limit, one associated with each open channel), while the subradiant states are perfectly decoupled from the external world.

The effective non-Hermitian Hamiltonian approach to open quantum systems was first formulated in a systematic way by in nuclear physics [4, 5], and provides a comprehensive and very general framework for studying open quantum systems in the regime of large as well as small opening, and at the superradiance crossover. For a closed discrete system with $N \times N$ Hamiltonian matrix $H_{j,k}$ that is coupled to a set of continuum channels labeled by c with couplings $A_j^c(E)$, the effective Hamiltonian for the discrete system is given by

$$H_{\rm eff}(E) = H + \Delta(E) - \frac{i}{2} Q(E)\,, \tag{1}$$

where

$$Q_{j,k}(E) = 2\pi \sum_c A_j^c(E) A_k^c(E)^* \rho^c(E)\,, \tag{2}$$

$$\Delta_{j,k}(E) = \sum_c P.V. \int dE' \frac{A_j^c(E') A_k^c(E')^* \rho^c(E')}{E - E'}\,, \tag{3}$$

and $\rho^c(E')$ is the density of states in channel c.

The Fourth Conference on Nuclei and Mesoscopic Physics 2014
AIP Conf. Proc. 1619, 64-72 (2014); doi: 10.1063/1.4899219

At this level no approximation has been made, i.e.,

$$G(E) = \frac{1}{E - H_{\rm eff}(E)} \tag{4}$$

is the exact Green's function for the discrete system, and fully takes into account the effect of the coupling to the external world. In practical applications, however, it is often convenient to neglect the energy dependence of the effective Hamiltonian and to approximate $H_{\rm eff}(E)$ as an $N \times N$ non-Hermitian matrix,

$$H_{\rm eff} \approx H + \Delta(E_0) - \frac{i}{2} Q(E_0) \tag{5}$$

for some suitable energy E_0 within the spectrum of $H_{\rm eff}$. We may then regard the N eigenvalues of $H_{\rm eff}$,

$$\mathscr{E}_r = E_r - \frac{i}{2}\Gamma_r, \tag{6}$$

as complex energies, corresponding to resonances centered at E_r with widths Γ_r. The regime of validity of this energy-independent approximation is discussed in Sec. 3 below.

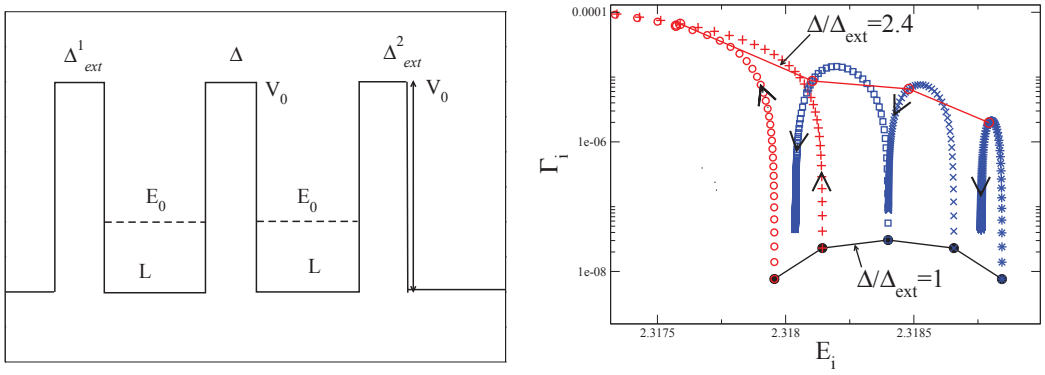

FIGURE 1. Left panel: A system of N square wells of width L, with neighboring wells separated by $N-1$ barriers of width Δ and the leftmost and rightmost wells separated from the outside by barriers of width $\Delta_{\rm ext}^{1,2}$, is illustrated for $N = 2$. All barriers have constant height V_0. Right panel: For $N = 5$ and the symmetric case $\Delta_{\rm ext}^1 = \Delta_{\rm ext}^2 \equiv \Delta_{\rm ext}$, the evolution of the five complex eigenvalues $\mathscr{E}_r$ of the effective Hamiltonian $H_{\rm eff}$ is shown as the coupling to the outside is increased by reducing the width of the external potential barrier width $\Delta_{\rm ext}$. The blue symbols are associated with the three subradiant resonances, whose resonance widths initially grow with increasing coupling starting from $\Delta_{\rm ext} = \Delta$, and then begin to decay at around $\Delta_{\rm ext} = \Delta/2.4$. The red symbols are associated with the two superradiant resonances, whose widths continue to grow past the superradiance crossover. For $N \to \infty$, the crossover can be shown to occur at $\Delta_{\rm ext} = \Delta/2$ [6, 7].

The non-Hermitian Hamiltonian formalism may be used to illustrate the superradiance transition in a simple but sufficiently realistic mesoscopic system, a sequence of one-dimensional wells separated by tunneling barriers. Specifically, we may consider a sequence of N square wells separated by $N-1$ barriers of height V_0 and width Δ, and with two additional barriers of width $\Delta_{\rm ext}^{1,2}$ on either side of the system separating the system from the outside. Such a potential is shown, for $N = 2$, in the left panel of Fig. 1. In the right panel, we see, for the case $N = 5$, the evolution in the complex plane of the five complex eigenvalues $\mathscr{E}_r$ associated with a single energy band centered on E_0 [6].

The superradiance phenomenon has profound implications for transport in open mesoscopic systems, as shown in Fig. 2, where the integrated transmission over an energy band $S = \int dE\, T(E)$ is plotted as a function of the opening size for openings that are symmetric (left panel) and asymmetric (right panel) [6, 8]. In contrast with classical transport, where transport efficiency increases monotonically with the size of the lead opening, here an optimal coupling is associated with the superradiance crossover. At stronger couplings, most of the decay width is shared by the two superradiant states, which are both localized at the two ends of the chain, and the remaining resonances are trapped, resulting in suppression of the transmission. In this simple model, the optimal opening associated with the superradiance peak may be computed analytically. Interesting real-world applications include, for example, efficiency of photosynthetic complexes and artificial light-harvesting devices, where efficiency may be maximized when the coupling to the reaction center corresponds to the superradiance peak [9].

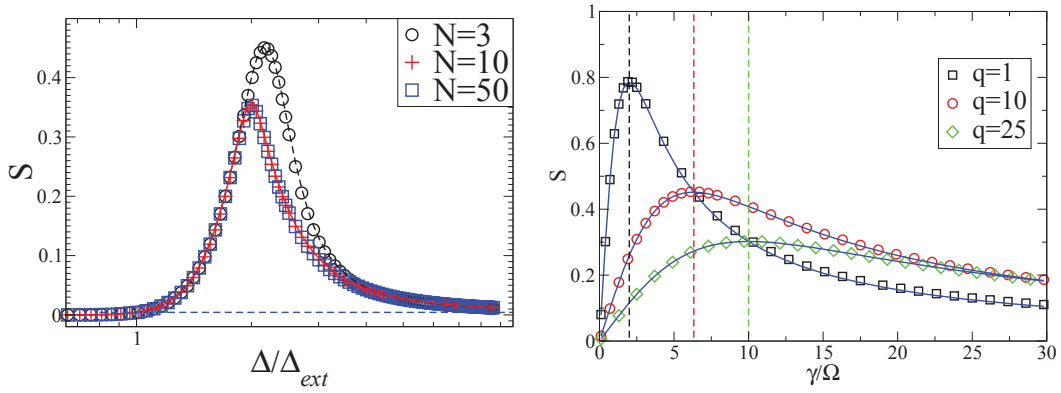

FIGURE 2. Left panel: The integrated transmission through a sequence of N potential wells (Fig. 1, left panel) is shown as the width of the external barriers $\Delta_{\rm ext}$ is varied, for several values of the system size N [6]. Here the opening is symmetric, $\Delta^1_{\rm ext} = \Delta^2_{\rm ext} \equiv \Delta_{\rm ext}$. Asymptotically, for $N \to \infty$, superradiance occurs at $\Delta_{\rm ext} = \Delta/2$. Right panel: Here, the chain length is fixed at $N = 100$ and asymmetric coupling to the outside is considered, $\Delta^1_{\rm ext} \neq \Delta^2_{\rm ext}$, with asymmetry parameter q being the ratio of the decay rates through the two external barriers. Here the transmission peak is predicted to occur at $\gamma/\Omega = 2\sqrt{q}$, where γ is the larger of the two decay rates and Ω is the inter-well coupling [8].

2. SUPERRADIANCE CROSSOVER AND THE LOCALIZATION TRANSITION IN DISORDERED CHAINS

Here we discuss the interplay of two important effects of quantum coherence: the superradiance phenomenon presented in Sec. 1 and Anderson localization that occurs at a critical strength of disorder [10]. For simplicity, instead of a physical potential such as discussed in Sec. 1, we may consider a tight-binding model of N sites. We begin with the one-dimensional Anderson model for a closed system [10, 2],

$$H = \sum_{j=1}^{N} E_j |j\rangle\langle j| + \Omega \sum_{j=1}^{N-1} \left(|j\rangle\langle j+1| + |j+1\rangle\langle j| \right), \tag{7}$$

where E_j are random and uniformly distributed in $[-W/2, +W/2]$. For $W = 0$, the eigenstates are extended (Bloch-like) states in an energy band $-2\Omega < E < 2\Omega$, whereas for $W > 0$ the system exhibits exponential localization $|\psi(j)| \sim \exp(-|j - j_0|/\xi)$, where $\xi \approx 96\,(1-(E/2\Omega)^2)(\Omega/W)^2$ for $W \ll \Omega$. Our interest, however, is in incorporating the coupling to the outside. As the simplest case, we choose a single continuum channel to which all N sites are coupled equally, so that $Q_{j,k}$ in Eq. (2) is a constant, $Q_{j,k} = \gamma$ for all j,k (physically, this corresponds to interaction with a field whose wavelength is large compared to the size of the system). For a wide band in the continuum (see Sec. 3), the real energy shift of Eq. (3) vanishes and we have

$$(H_{\rm eff})_{j,k} = H_{j,k} - i\frac{\gamma}{2}. \tag{8}$$

The relevant dimensionless parameter characterizing the size of the opening is

$$\kappa = \gamma/D, \tag{9}$$

where D is mean level spacing. In particular in the clean limit ($W/\Omega \ll 1$) we have $\kappa = \gamma N/\pi\sqrt{(2\Omega)^2 - E^2}$, while in the opposite limit of strong disorder the mean level spacing is dominated by the disorder, and so $\kappa = \gamma N/W$.

For a small opening, $\kappa \ll 1$, H dominates in Eq. (8) and the effect of the opening is a perturbation with eigenvalues acquiring small imaginary parts. On the other hand, for a large opening, $\kappa \gg 1$, the dominant term in the effective Hamiltonian (8) is the second term, which has one eigenstate $|d\rangle = \frac{1}{\sqrt{N}}(1,\ldots,1)^T$ with eigenvalue $-i\gamma N/2$ (the doorway state), while the remaining eigenstates have eigenvalue 0. Thus, we see that in the limit $\kappa \to \infty$, the superradiant eigenstate approaches the doorway state and the remaining $N-1$ eigenstates are trapped inside the closed system, with vanishing decay widths.

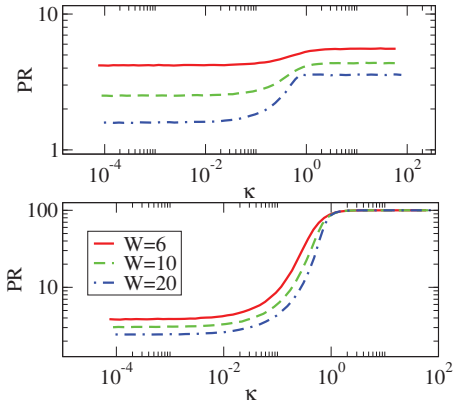

FIGURE 3. The participation number PR in the open Anderson model ($N = 100$) is calculated as a function of the openness parameter κ for the superradiant state, defined as the state with the largest width (upper panel) and for the remaining $N-1$ subradiant states (lower panel). Results are shown for several disorder strengths W, in units where $\Omega = 1$ [11].

To investigate quantitatively the effect of the superradiance transition on eigenstate localization, we compute in Fig. 3 the average participation number $PR = \overline{\left(\sum_j |\langle j|\psi\rangle|^4\right)^{-1}}$ for the superradiant state, defined as the state with the largest width (upper panel) and for the remaining $N-1$ subradiant states (lower panel), as a function of the openness parameter κ. Here we are in the Anderson localized regime $W/\Omega \gg 1$. We see that for weak opening ($\kappa \ll 1$) the PR is indistinguishable for the superradiant and subradiant states (and is given as a function of disorder by the standard Anderson theory). In the opposite limit, for $\kappa \gg 1$, the PR approaches N for the superradiant state (indicating complete delocalization), while the PR for the subradiant states also increases, but only by an $O(1)$ factor.

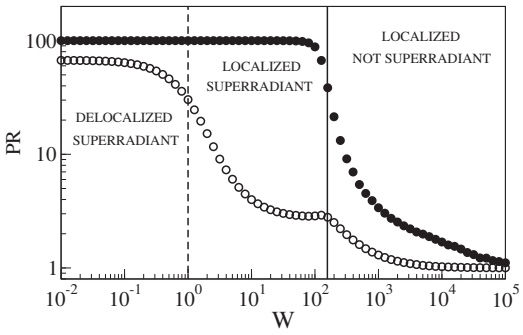

FIGURE 4. The participation number PR in the open Anderson model ($N = 100$) is calculated as a function of the disorder strength W for $\gamma = \Omega = 1$. Black and white circles represent the superradiant and subradiant states, respectively [11].

To study the Anderson and superradiance crossovers in a single plot, we may fix the opening size γ and vary the disorder strength, as in Fig. 4. Starting from the right side of the figure, we notice that for sufficiently strong disorder W (in units $\Omega = 1$), the system is localized and $\kappa = N/W \ll 1$, so we are in the weakly open regime, where superradiant and subradiant states coincide. This is the "localized, not superradiant" regime. At $W = N$ (here $N = 100$), $\kappa = 1$ and the system goes through a superradiance crossover, where the superradiant state is separated from the others and delocalizes completely (approaching the doorway state). Finally, for $W < 1$, the disorder becomes weak and all states become delocalized (the Anderson crossover); the system however is still superradiant and the superradiant state with $PR = N$ is clearly distinguishable from the Bloch-like subradiant states with $PR = 2N/3$.

Analytical results for the open Anderson model may be obtained in limiting cases of weak and strong opening, and these results may be extended to other models with different closed-system Hamiltonians H and different forms of the coupling. For example, when the opening is small compared to the disorder strength ($\kappa \ll 1$), the typical eigenstates

are given by first-order perturbation theory in $\kappa = \gamma/(W/N)$,

$$|n\rangle = \frac{1}{\sqrt{C_n}}\left[|n^0\rangle - \frac{i}{2}\sum_{k^0\neq n^0}\frac{\langle k^0|Q|n^0\rangle}{E_{n^0}-E_{k^0}}|k^0\rangle\right], \tag{10}$$

where $|n^0\rangle$ are eigenstates of the closed Anderson model, $Q_{j,k} = \gamma$ in the site basis and C_n is a normalization constant. Thus, the typical open-system eigenstate $|n\rangle$ is dominated by a single Anderson eigenstate of the closed system, $|n_0\rangle$, with $O(\kappa^2)$ admixture of a few other Anderson states that are nearby in energy ($E_{n^0} - E_{k^0} \sim W/N$). The participation number PR is dominated by an $O(\kappa)$ fraction of Anderson eigenvalue pairs with energy spacing less than γ, yielding $PR(\kappa) = PR(0) + O(\kappa)$, where $PR(0)$ is the participation number of the closed system (in this case, the Anderson model) [11].

In the opposite case of large opening, it is the opening that dominates the full effective Hamiltonian, and the closed system contribution H must be regarded as a perturbation. Here we may follow the approach of Ref. [12] and perform (degenerate) perturbation theory in $1/\kappa$. We obtain for the superradiant state

$$|SR\rangle = \frac{1}{\sqrt{C}}\left[|d\rangle + \frac{1}{\kappa\sqrt{3(N-1)}}\sum_{\mu=1}^{N-1}\frac{r_\mu}{i-2\tilde{\varepsilon}_\mu/\gamma N}|\mu\rangle\right], \tag{11}$$

where $|\mu\rangle$ are the subradiant states in the limit of infinite opening (i.e., states orthogonal to the doorway state $|d\rangle$), $\tilde{\varepsilon}_\mu$ are the eigenvalues of H restricted to the subradiant subspace, the r_μ are random coefficients satisfying $\overline{r_\mu^2} = 1$, and C is a normalization constant. Thus, the superradiant $|SR\rangle$ contains an $O(1/\kappa^2)$ admixture of non-doorway states for large κ. Similarly, the subradiant states are given as

$$|SUB_\mu\rangle = \frac{1}{\sqrt{C'_\mu}}\left[|\mu\rangle - \frac{1}{\kappa\sqrt{3(N-1)}}\frac{r_\mu}{i-2\tilde{\varepsilon}_\mu/\gamma N}|d\rangle\right], \tag{12}$$

so that each subradiant state contains an $O(1/N\kappa^2)$ admixture of the doorway state for large κ. Importantly, we note that the states $|\mu\rangle$ depend on H and are sensitive to the degree of disorder, whereas the doorway $|d\rangle$ is disorder-independent and depends only of the form of the coupling to the outside world. Thus, in the superradiant regime, disorder tends to localize the subradiant states while the superradiant state is left unaffected, consistent with the numerical results in Fig. 4.

Analogous results, not presented here, have been obtained in three-dimensional Anderson models [13].

3. REGIME OF VALIDITY OF THE ENERGY-INDEPENDENT EFFECTIVE HAMILTONIAN APPROXIMATION

We have seen above that the approximation (5) replaces the exact system propagator, which fully takes into account the coupling to the continuum, with a finite matrix H_{eff}. In other words, an infinite-dimensional system is reduced to a finite-dimensional one. This of course greatly simplifies the investigation of an open quantum system, both analytically and numerically, but it is important to understand whether such a drastic approximation may actually be valid in non-trivial situations. For this purpose we consider a simple model consisting of a ring coupled to a lead, as pictured in Fig. 5 (left panel). Models of this type have been considered by multiple authors [14, 15, 16, 17, 18, 19] to describe different systems, such as molecular J-aggregates [20], bio-inspired devices for photon sensing [15], and efficient light harvesting systems [16]. In particular they have been often considered in the framework of exciton transport in natural photosynthetic systems, such as LHI and LHII, where chlorophyll molecules aggregate in ring-like structures [21].

The system pictured in Fig. 5 (left panel) consists of N_R sites on the ring (labeled $1 \ldots N_R$) and N_L sites in the lead (labeled $N_R + 1 \ldots N_R + N_L$). The Hamiltonian of the full system is taken to be

$$H = H_R + V_{RL} + H_L\,. \tag{13}$$

Here

$$H_R = \sum_{j=1}^{N_R} E_j|j\rangle\langle j| + \Omega\sum_{j=1}^{N_R-1}(|j\rangle\langle j+1| + h.c.) + \Omega\,(|N_R\rangle\langle 1| + h.c.) \tag{14}$$

is the Hamiltonian of the N_R-site ring, and on-site energies E_j may be uniformly distributed in $[-W/2, W/2]$, as in the Anderson model, although we will initially set $W = 0$. The lead, consisting of a chain of N_L sites, is described by the Hamiltonian

$$H_L = \Omega_L \sum_{j=N_R+1}^{N_R+N_L-1} (|j\rangle\langle j+1| + h.c) \,. \tag{15}$$

Finally, the ring-lead coupling is

$$V_{RL} = \Omega_{RC} \sum_{i=1}^{N_R} (|i\rangle\langle N_R+1| + h.c.) \,, \tag{16}$$

i.e., all sites on the ring are coupled equally to the lead, as in the simple model presented in Sec. 2.

In the limit $N_L \to \infty$, the spectrum in the lead is continuous, and following the prescription described in Sec. 1 for constructing the $N_R \times N_R$ effective Hamiltonian for the ring system (treating the lead as the outside), we have

$$Q_{j,k}(E) = 2\pi A_j(E)(A_k(E))^* \rho(E) = \frac{2\Omega_{RC}^2}{\Omega_L} \sqrt{1-(E/2\Omega_L)^2} \,. \tag{17}$$

The energy dependence arises both from the ring-lead couplings $A_j(E)$ and the lead density of states $\rho(E)$. However, we see that for large Ω_L, compared with the spectrum of the ring Hamiltonian H_R (i.e., $\Omega_L \gg \Omega$ in the clean case), the energy dependence may be neglected and we have $Q_{j,k} = 2\Omega_{RC}^2/\Omega_L$. Similarly, the real energy shift $\Delta(E)$ (Eq. (3)) is seen to vanish in this limit and we obtain the energy-independent non-Hermitian Hamiltonian for the ring:

$$H_{\rm eff} = H_R - \frac{i}{2} Q, \quad Q_{j,k} = \gamma \equiv \frac{2\Omega_{RC}^2}{\Omega_L} \,, \tag{18}$$

as shown in Fig. 5 (right panel).

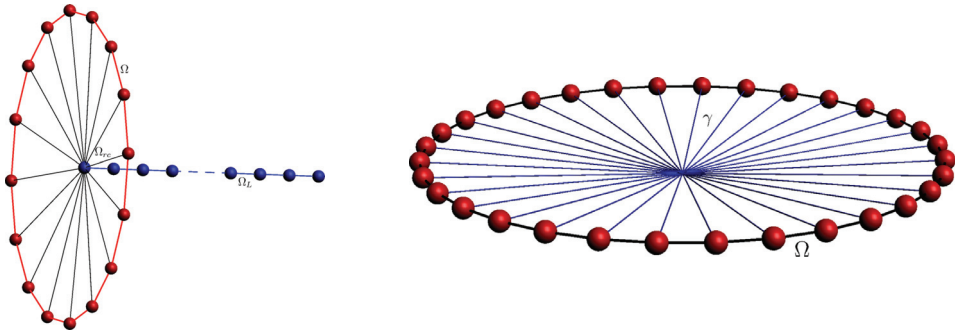

FIGURE 5. Left panel: The model described by the Hermitian Hamiltonian given in Eq. (13). Right panel: The model described by the effective non-Hermitian Hamiltonian given in Eq. (18).

Note that the Hermitian matrix Q in Eq.(18) has only one non-zero eigenvalue (N_R), and for the clean case ($W = 0$), Q commutes with H_R. This implies that for any $\gamma \neq 0$ we are in a superradiant regime with only one superradiant state given by the fully symmetric state:

$$|SR\rangle = \frac{1}{\sqrt{N_R}} \sum_{k=1}^{N_R} |k\rangle \quad \text{with} \quad \mathscr{E}_{SR} = 2\Omega - iN_R\gamma/2 \,. \tag{19}$$

All other states are subradiant for any γ and are perfectly trapped (having zero decay widths).

We may now explicitly compare the dynamics predicted by the effective non-Hermitian Hamiltonian for the ring, Eq. (18), with the dynamics obtained from the exact Hermitian model than includes the entire ring and lead system, Eq. (13). Both calculations are performed in the absence of disorder ($W = 0$). In Fig. 6 we show the survival probability (probability to remain in the ring)

$$P(t) = \sum_{k=1}^{N_R} |\langle k|\psi(t)\rangle|^2 \tag{20}$$

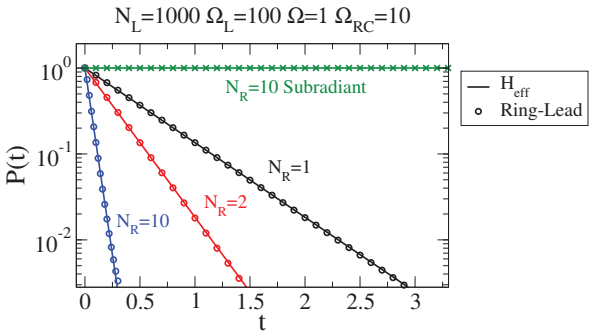

FIGURE 6. The survival probability $P(t)$ is computed using the exact Hermitian Hamiltonian, Eq. (13) (symbols) and the non-Hermitian model, Eq. (18) (solid lines). The horizontal line (with crosses) is obtained starting with an antisymmetric initial state $|\psi_0\rangle = \sum_{k=1}^{N_R}(-1)^k|k\rangle$, while the remaining three data sets are obtained starting from the superradiant state $|SR\rangle$, with different numbers of sites on the ring. Here we have fixed $\Omega = 1$, $\Omega_{RL} = 10$, $\Omega_L = 100$, and $N_L = 1000$.

for a excitation located in the ring at $t = 0$. We easily see the superradiance effect when starting in state $|SR\rangle$, with the decay rate being proportional to the number of sites on the ring. We also see perfect agreement between the exact calculation and the non-Hermitian Hamiltonian approximation. Clearly for larger times the two models will disagree due to the fact that in our simulations both Ω_L and N_L are finite. We have checked that upon increasing both parameters the agreement time also increases, see Fig. 7 (left panel). Note that for the chosen parameters the bounce time $t_b = N_L/\Omega_L$ (the time for the excitation to reach the end of the lead and return to the ring) is much larger then the simulation time.

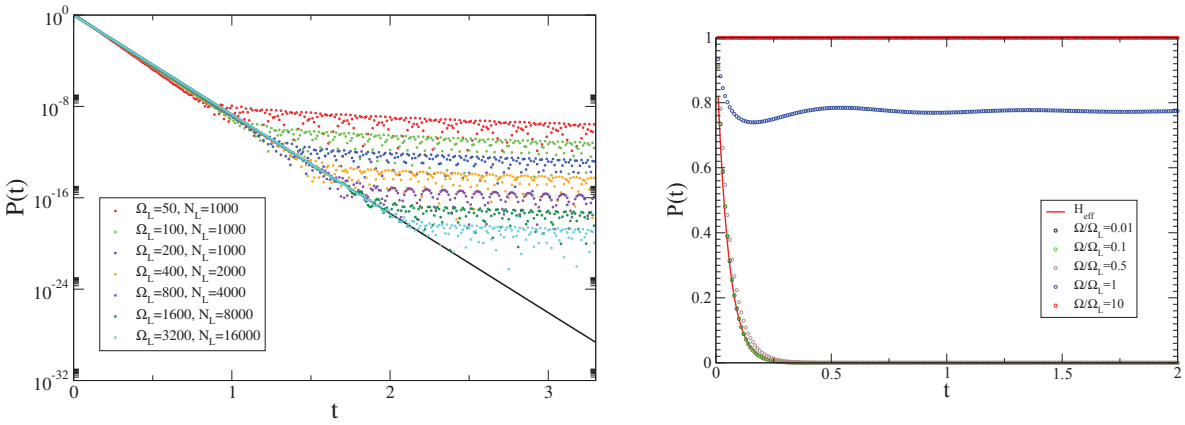

FIGURE 7. The survival probability, $P(t)$, is plotted starting from the superradiant state $|SR\rangle$ at $t = 0$. Each set of dots or circles represents a calculation obtained with the full Hermitian model, Eq. (13), and the solid line or curve in each panel is the result obtained with the effective Hamiltonian, Eq. (18), with $\gamma = 2\Omega_{RC}^2/\Omega_L$. Left panel: $\Omega = 1$ and $N_R = 10$ are fixed, while Ω_L and Ω_{RC} are varied keeping $\gamma = 2\Omega_{RC}^2/\Omega_L$ constant. Right panel: $N_R = 10$, $N_L = 100$, $\Omega_L = 100$, and $\Omega_{RC} = 10$ are fixed, and Ω is varied.

To see the limitations of the energy-independent approximation, in Fig. 7 (right panel) we vary the hopping parameter Ω, which controls the width of the density of states in the ring. We see that when $\Omega/\Omega_L \ll 1$, so that the ring spectrum is very narrow compared to spectral width in the lead, the energy-independent non-Hermitian Hamiltonian provides an excellent approximation, for $\Omega = \Omega_L/2$ small but noticeable deviations occur, and for $\Omega \geq \Omega_L$, the energy-independent approximations fails entirely, as expected.

Finally we consider the situation in the presence of disorder. In Fig. 8, we compute the efficiency of transport to the lead, defined as $1 - P(t = 1/\gamma)$, as a function of the disorder strength W. Here the ring spectrum has range $[-W/2, W/2]$ while the lead spectrum has range $[-2\Omega_L, 2\Omega_L]$ and indeed very good agreement between the exact calculation and the energy-independent approximation is observed when $W < 4\Omega_L$.

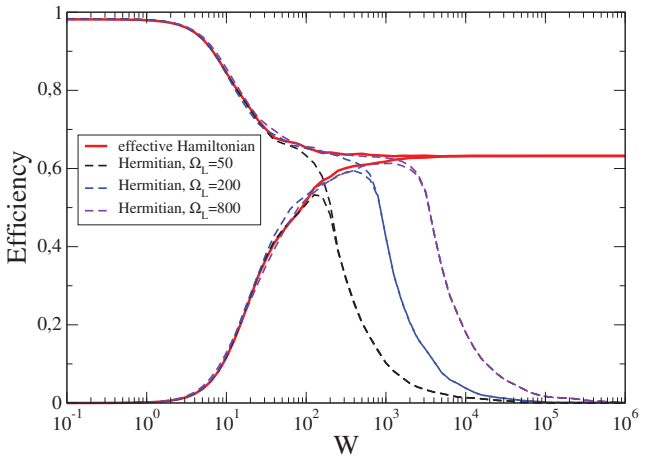

FIGURE 8. The transport efficiency $1-P(t=1/\gamma)$ is calculated as a function of disorder strength W, for several values of the lead parameter Ω_L. The dashed curves are computed using the exact Hermitian Hamiltonian, Eq. (13), while the solid red curves are computed using the energy-independent non-Hermitian approximation, Eq. (18). The three dashed curves with high efficiency as $W \to 0$ correspond to the symmetric initial state, $N_R^{-1}\sum_{k=1}^{N_R}|k\rangle$, while the three dashed curves that approach zero efficiency as $W \to 0$ correspond to the antisymmetric initial state, $N_R^{-1}\sum_{k=1}^{N_R}(-1)^k|k\rangle$. The parameters used are $N_R=4$, $\Omega=1$, $\gamma=2$, and $N_L=\Omega_L$ (so that $t=1/\gamma<t_b$ and bounce effects need not be considered) and an average is performed over 100 realizations of the disorder.

4. CONCLUSIONS AND OUTLOOK

Superradiance is an effect of quantum coherence with important implications for resonance structure and transport in mesoscopic open systems. We have seen that the non-Hermitian Hamiltonian method provides a powerful tool for studying, both analytically and numerically, the behavior of open quantum systems without assuming that the coupling to the outside is small. In particular, the method provides a framework for analyzing the superradiance crossover in a quantum system as the strength of its coupling to the external world is varied.

In Sec. 2 we have studied the interplay of openness and disorder in a paradigmatic disordered system, the Anderson model. In addition to the usual localization transition present in closed quantum systems, here a transition to a superradiant regime is shown to occur as either the disorder strength or the coupling to the outside is varied. As an effect of openness, the structure of eigenstates undergoes a strong change in the superradiant regime: we show that the sensitivity to disorder of the superradiant and the subradiant subspaces is very different. Specifically, superradiant states remain delocalized as disorder increases, while subradiant states are strongly sensitive to the degree of disorder. A number of important questions remain concerning the degree to which the qualitative features of the superradiance crossover may be sensitive both to the details of the closed-system intrinsic Hamiltonian H (in this case, the Anderson model) and to the form of the coupling to the outside (here, all sites were coupled equally to a single channel). Specifically, since the superradiance criterion involves comparing the coupling strength to the level spacings of the intrinsic Hamiltonian H, the relevant properties of H should include both the spectral statistics (spacing distribution) and the overall shape of the spectrum. Similarly, the effect of the opening is expected to depend on the structure of the doorway state (in the eigenbasis of H). These interrelated questions are currently under investigation.

In Sec. 3 we have explored the validity of the energy-independent non-Hermitian Hamiltonian approximation in a simple model of a ring coupled to a lead, and the preliminary results presented here strongly suggest that the approximation is reliable as long as the range of the effective Hamiltonian spectrum is small compared to the width of the spectrum in the lead. This condition is of course the same as the one underlying the Fermi Golden Rule, and indeed the effective non-Hermitian Hamiltonian approximation may usefully be regarded as a matrix generalization of the Fermi Golden Rule. This connection will be explored more fully elsewhere [22]. In the future, it will be useful to consider effects going beyond the energy-independent non-Hermitian Hamiltonian approximation, taking systematically into account leading corrections due to the energy-dependence of the coupling to the continuum and of the continuum density of states.

ACKNOWLEDGMENTS

This work was supported in part by the U.S. National Science Foundation under Grant. No. PHY-1205788.

REFERENCES

1. C. W. Beenakker, Rev. Mod. Phys. **69**, 731 (1997).
2. P. A. Lee and T. V. Ramakrishnan, Rev. Mod. Phys. **57**, 287 (1985).
3. R. H. Dicke, Phys. Rev. **93**, 99 (1954).
4. C. Mahaux and H. A. Weidenmüller, *Shell Model Approach to Nuclear Reactions* (North Holland, Amsterdam, 1969).
5. V. V. Sokolov and V. G. Zelevinsky, Ann. Phys. (N.Y.) **216**, 323 (1992).
6. G. L. Celardo and L. Kaplan, Phys. Rev. B **79**, 155108 (2009).
7. C. Pacher and E. Gornik, Phys. Rev. B **68**, 155319 (2003).
8. G. L. Celardo, A. M. Smith, S. Sorathia, V. G. Zelevinsky, R. A. Sen'kov, and L. Kaplan, Phys. Rev. B **82**, 165437 (2010).
9. G. L. Celardo, F. Borgonovi, V. I. Tsifrinovich, M. Merkli, and G. P. Berman, J. Phys. Chem. C **116**, 22105 (2012).
10. P. W. Anderson, Phys. Rev. **109**, 1492 (1958).
11. G. L. Celardo, A. Biella, L. Kaplan, and F. Borgonovi, Fortschr. Phys. **61**, No. 2-3, 250-260 (2013).
12. V. V. Sokolov, I. Rotter, D. V. Savin, and M. Müller, Phys. Rev. C **56**, 1031 (1997).
13. A. Biella, F. Borgonovi, R. Kaiser, and G. L. Celardo, Eur. Lett. **103**, 57009 (2013).
14. J. M. Moix, M. Khasin, and J. Cao, New J. Phys. **15**, 085010 (2013).
15. K. D. B. Higgins, S. C. Benjamin, T. M. Stace, G. J. Milburn, B. W. Lovett, and E. M. Gauger, arXiv:1306.1483.
16. M. Sarovar and K. B. Whaley, New J. Phys. **15**, 013030 (2013).
17. A. Olaya-Castro, C. F. Lee, F. Fassioli Olsen, and N. F. Johnson, Phys. Rev. B **78**, 085115 (2008).
18. J. Grad, G. Hernandez, and S. Mukamel, Phys. Rev. A **37**, 3835 (1988); F. C. Spano, J. R. Kuklinski and S. Mukamel, J. Chem. Phys. **94**, 7534 (1991); M. J. Stephen, J. Chem. Phys. **40**, 669 (1964); R. H. Lehmberg, Phys. Rev. A **2**, 883 (1970).
19. F. C. Spano and S. Mukamel, J. Chem. Phys. **91**, 683 (1989).
20. H. Fidder, J. Knoester, and D. A. Wiersma, J. Chem. Phys. **95**, 7880 (1991); J. Moll, S. Daehne, J. R. Durrant, and D. A. Wiersma, J. Chem. Phys. **102**, 6362 (1995).
21. X. Hu, T. Ritz, A. Damjanovic, and K. Schulten, J. Phys. Chem. B **101**, 3854 (1997).
22. G. L. Celardo, in preparation.